Computers and Geotechnics 84 (2017) 58–67

Contents lists available at ScienceDirect

Computers and Geotechnics

journal homepage: www.elsevier.com/locate/compgeo

Research Paper

DEM investigation of the effect of intermediate principle stress on particle breakage of granular materials

Yiming Liu [a], Huabei Liu [a,*], Haijun Mao [b]

[a] School of Civil Engineering and Mechanics, Huazhong University of Science and Technology, 1037 Luoyu Road, Wuhan, Hubei 430074, China
[b] Institute of Rock and Soil Mechanics, Chinese Academy of Sciences, Xiaohongshan, Wuhan, Hubei 430071, China

ARTICLE INFO

Article history:
Received 5 August 2016
Received in revised form 20 October 2016
Accepted 24 November 2016

Keywords:
Discrete element method
Particle breakage
Intermediate principle stress
Total energy input

ABSTRACT

This study investigates the influence of the intermediate principle stress on the particle breakage of granular materials. The crushable agglomerate method is applied to model soil particles and numerical true triaxial tests were carried out. The results show that particle breakage increases with increasing b value, the relationship of which follows an exponential function and agrees well with previous experimental results. More importantly, the study found that the relationship between particle breakage and total energy input is independent of the intermediate principle stress, which provides a good basis for the constitutive modeling of granular materials.

1. Introduction

Particle crushing has an essential influence on the important engineering properties of granular materials, such as stress-strain relationship, strength, volume change, and yielding [1,2]. This is because a change in particle size distribution due to particle crushing may create a very drastic change in the internal structure [3]. Due to its importance, particle crushing behavior of granular materials has been investigated by a number of researchers. Single particle crushing behavior has been investigated using uniaxial compression tests [4–10], based on which and together with fracture theory, theoretical criteria for particle breakage have been proposed [11–15]. Triaxial tests have been carried out to study the effect of particle breakage on the mechanical behavior of granular materials [2,16–27]. To investigate the effect of particle breakage on the mechanical behavior of granular materials, various breakage indices have been proposed [1,16,25,28]. Based on the experimental results, constitutive models have been developed to take into account the influence of particle breakage in continuum numerical analyses [26,29–32]. Discrete element method has also been applied to investigate the behavior of crushable granular materials, which has brought the investigation of particle breakage into a grain scale and has provided many new insights [3,13–15,33–39].

Previous studies show that particle crushing of granular materials is affected by many factors, including the relative density, stress level, loading path, particle strength, mineral composition, particle shape, and particle size distribution [40]. Among all these factors, the effect of intermediate principle stress on particle breakage has not been fully clarified. Some limited study showed that particle breakage is dependent on the intermediate principle stress ratio b [21], however, the mechanism of the effect of b on particle breakage is still not clear. This may be due to the difficulties of carrying out experimental research on particle breakage considering complex stress path. The type of soil, testing conditions, boundary conditions and instrumental limitations may lead to difficulties in revealing the hidden mechanism [40]. Previous experimental studies showed that particle breakage is very well correlated with the external work, or the total energy input, applied to the soil element [1,2,20,23,32,41], but these tests only covered simple stress paths such as triaxial compression, and the influence of intermediate stress is still not known [20,23]. However, it is very difficult to track the evolutions of particle breakage and input work in true triaxial tests, which is essential to understand the mechanics of particle breakage.

DEM can overcome the limitation encountered in experimental true triaxial test studies, because it enables one to prepare the exact same sample in each numerical experiment for a certain b value without any bias in the initial fabric [40]. Furthermore, with the development of particle breakage simulation method using DEM, it is possible to fully understand the mechanism of the effect of b on particle breakage.

* Corresponding author.
E-mail addresses: yiming_liu@hust.edu.cn (Y. Liu), hbliu@hust.edu.cn (H. Liu), hjmao@whrsm.ac.cn (H. Mao).

http://dx.doi.org/10.1016/j.compgeo.2016.11.020
0266-352X/

This study explores the effect of intermediate principle stress on particle breakage of granular materials. Crushable agglomerate method was used to model realistic particle grains of granular materials. Single agglomerate uniaxial compression tests were conducted to ensure that the particle strength follows Weibull's distribution. Then, a series of true triaxal tests were simulated. The effect of intermediate principle stress ratio on the mechanical behavior was analyzed and compared with previous experimental results. Two breakage indices were used to explore the relationship between particle breakage and intermediate principle stress ratio. The relationships between particle breakage and total energy input under different loading paths are also discussed.

2. DEM simulations

2.1. DEM method and contact models

The commercial DEM software PFC3D3.1 was used to investigate the particle breakage behavior of granular materials in this study. The PFC3D software uses the "soft contact" approach, which assumes that all spheres are rigid and can't change their shape and size, and inter-action of spheres is represented by assigning each sphere a stiffness and allowing them to overlap. The constitutive models used in this study are the same as those in Wang and Yan [37]. A brief description of the models is given in the following. A linear contact stiffness model, a Mohr-Coulumb based slip model and a parallel bond model are introduced to represent the constitutive contact behavior between contacting spheres. In the linear contact stiffness model, the force-displacement relationships for the normal and tangential component models are given by

$$F_i^n = K^n \cdot u_i^n \tag{1}$$

$$\Delta F_i^s = -K^s \cdot \Delta u_i^s \tag{2}$$

where K^n and K^s are the stiffnesses of normal and tangential model, respectively. The contact stiffness is computed assuming that the stiffnesses of the two contacting spheres act in series, so that K^n and K^s are defined by following equations:

$$K^n = \frac{k_n^{[A]} \times k_n^{[B]}}{k_n^{[A]} + k_n^{[B]}} \tag{3}$$

$$K^s = \frac{k_s^{[A]} \times k_s^{[B]}}{k_s^{[A]} + k_s^{[B]}} \tag{4}$$

where the superscripts [A] and [B] denote the two spheres in contact.

The slip model describes the constitutive behavior tangential to the particle contact between two particles. It is defined by the friction coefficient at the contact μ, where μ is taken to be the friction coefficient of the two contacting entities. The slip model starts working at the contact *i*, when the following condition is satisfied:

$$|F_i^s| \geqslant \mu \cdot |F_i^n| \tag{5}$$

where F_i^s is the contact tangential force and F_i^n is the contact normal force.

The bond model used in this study is parallel bond. The parallel bond can be imagined as an elastic circular disk lying on the contact plane and centered at the contact point, which acts like a beam. This makes the parallel bond able to transmit both transmit both forces and moments between particles. Each parallel bond has normal and shear stiffness (in terms of stress/displacement), normal and shear strength (in terms of stress) and a radius. The load-deformation-relationships for tension and compression, bending, shear and torsion are linear. The load bearing capacity is calculated as the elastic bearing capacity of a cylindrical beam. The radius of a parallel bond can be calculated by a predefined radius ratio multiplying the radius of the smaller spheres in the contact.

2.2. Crushing test of single crushable agglomerates

2.2.1. Crushable agglomerate modeling

The appropriate approach to model a realistic crushable granular grain is essential to study the shear behavior of an assembly of crushable particles. Crushable agglomerate method which is firstly developed by Robertson and Bolton [33], then used by many investigators [3,34–39], is found to be an effective approach for simulating realistic crushable particles. In this method, crushable agglomerates are composed by a large number of elementary, uncrushable spheres, which are bonded together by breakable bonds. Each elementary sphere is given a certain probability of existence to provide the statistical variation of the strength and shape of agglomerates.

In this study, the crushable agglomerate method by Robertson and Bolton [33] is adopted. However, the contact bond model applied in the original method is replaced by parallel bond model, because the contact bond model fails to consider rotational resistance, which frequently leads to the absence of a clear and visible physical fracture of an agglomerate [37]. The proportion of removed balls is set as 10% in this study, in order to obtain smooth stress-strain relationships. The parameters used in this study are shown in Table 1. The parameters of linear contact stiffness model are from Cheng et al. [34]. The parameters of parallel bond model are based on those in Wang and Yan [37] and Laufer [38], but parametric analyses were carried out to determine the final values to ensure smooth stress-strain relationships in the numerical tests.

2.2.2. Crushing of a single agglomerate

A realistic granular particle may have many flaws, and its fracture strength under compression tests is determined by the number and size of these flaws. As a result, the fracture strength of granular particles may vary widely. The Weibull's statistical distribution is found to be a useful tool to describe the variation of fracture strength of crushable granular particles [7,8]. Robertson and Bolton [33] firstly developed an agglomerate method using PFC3D to model such strength variation of granular materials by randomly removing balls or weakening bonds.

In this study, 30 agglomerates, which consisted of about 57 elementary balls, were created by giving each elementary ball a probability of existence of 90%. The diameter of each elementary ball was 0.5 mm. Then compression tests were conducted on these agglomerates. The fracture strengths of these agglomerates were analyzed using Weibull's distribution as:

$$P_s = exp\left[-\left(\frac{\sigma}{\sigma_0}\right)^m\right] \tag{6}$$

Table 1
Parameters of crushable agglomerates.

Density of ball (kg/m^3)	2600
Normal and shear stiffness of ball (N/m)	4.0e6
Friction coefficient μ of ball	0.5
Normal and shear parallel bond strength (N/m^2) after shearing	1.0e8
Normal and shear parallel bond strength (N/m^2) before shearing	2.0e12
Normal and shear parallel bond stiffness (N/m^3)	4.0e12
Ratio of parallel bond radius to ball radius	0.5
Normal and shear stiffness of wall (N/m)	4.0e8
Friction coefficient between walls and balls	0.0
Percentage of spheres removed at random (%)	10

where P_s is the survival probability of a particle with size d, σ is the induced tensile stress, and σ_0 is the characteristic tensile stress at which 37% of tested particle survive, and m is the Weibull's modulus.

The survival probabilities P_s of 30 agglomerates are calculated using the mean rank position proposed by Davidge [42] as follow:

$$P_s = 1 - \frac{i}{N+1} \tag{7}$$

in which i is the rank position of an agglomerate when sorted into increasing order of equivalent stress, and the N is the number of agglomerates, which is 30 in this study.

To estimate the Weibull modulus, Eq. (6) can be rewritten as:

$$\ln\left[\ln\left(\frac{1}{P_s}\right)\right] = m\ln\left(\frac{\sigma}{\sigma_0}\right) \tag{8}$$

Fig. 1 presents the relationships between the fracture strength and the survival probability P_s for agglomerates tested in this study. Fig. 1 illustrates that the results obtained from DEM agglomerates is in good agreement with Weibull's distribution. The Weibull's modulus is approximately 2.186, and the characteristic fracture stress σ_0 is 80.65 MPa.

2.3. True triaxial compression test

2.3.1. Specimen preparation

The numerical cubical specimens have an initial dimension of 30mm enclosed by six rigid, frictionless walls. A set of 582 "exo-spheres" following a designed particle size distribution shown in

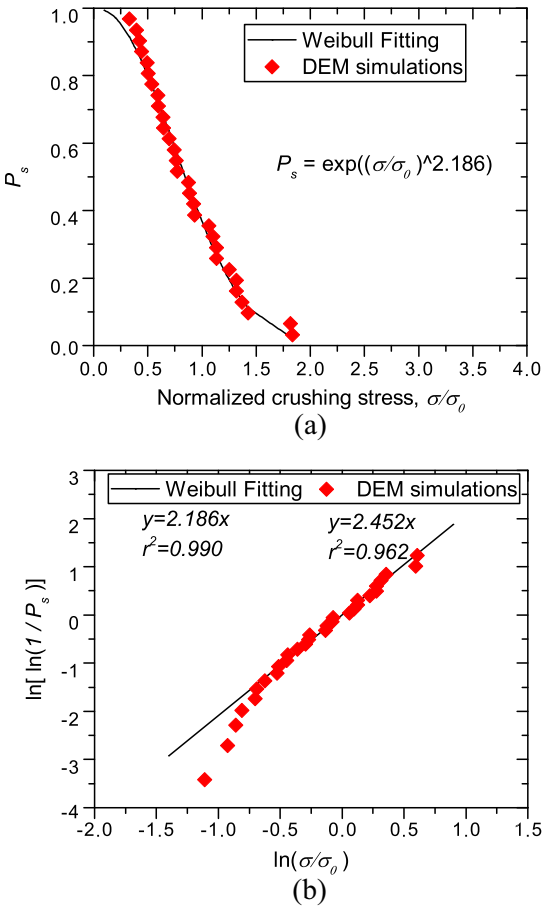

Fig. 1. Survival distribution curve of singe agglomerate crushing: (a) normalized distribution; (b) Weibull modulus.

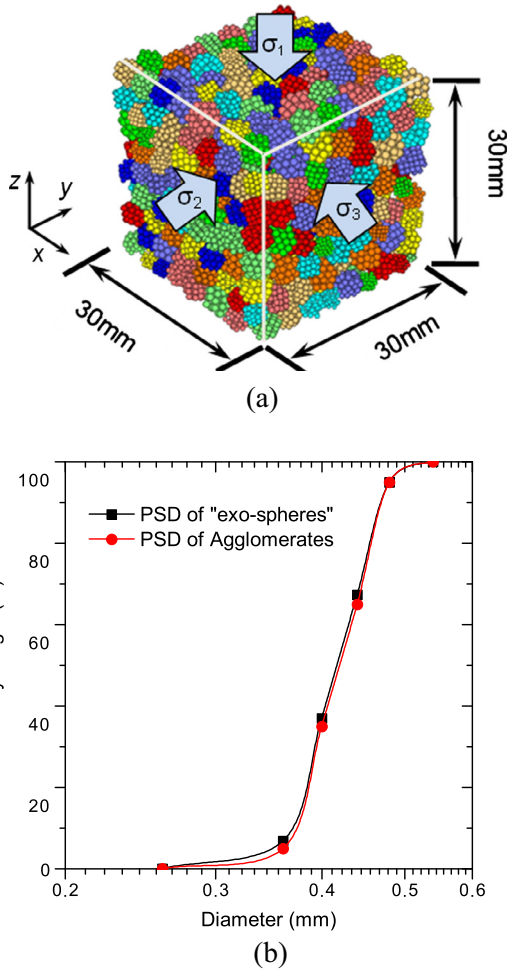

Fig. 2. Configuration of cube model and Particle size distribution: (a) numerical simple; (b) particle size distribution.

Fig. 2(b) were first created using the radius expansion method. Then a linked list storing the radii of these exo-spheres and the coordinates of their centres were created. After that, randomly rotated crushable agglomerates were created to replace the exo-spheres. The agglomerates centred at the coordinates in the linked list. The radii of elementary spheres in the agglomerates were set to 1/5 of the replaced exo-spheres, and each elementary sphere had a survival probability of 90%. Then the assembly of crushable agglomerates was cycled to equilibrium. The finial specimen is shown in Fig. 2(a), and its PSD was presented in Fig. 2(b) as PSD of the agglomerates. The parallel bond strength was set to a relatively high value of 2×10^{12} N/m^2 in order to ensure no bond breakage occurring during isotropic compression. Similar approach was adopted in Kwok and Bolton [36].

2.3.2. Isotropic compression

After the specimen was created, it was isotropically compressed to a given confining stress. A servo algorithm was employed to make sure this process was stable and controllable and a complete equilibrium condition was achieved. In each step, the stress in each direction was calculated and compared with confining stress, then the velocity was calculated and applied to corresponding walls. The confining stresses used in this study were 400 kPa, 600 kPa, 800 kPa, and 1000 kPa, respectively.

2.3.3. True triaxial compression

After the designed confining stress condition was reached, the specimen was then sheared by moving the walls in the z direction towards each other at a constant velocity of 0.05 m/s. A new servo algorithm was employed at this stage. The servo control on the walls in the z-direction was dismissed and a constant small velocity of 0.05 m/s was applied to these two walls so that they moved towards each other. The servo control on the walls in the x-direction did not change, while that on the walls in the y-direction was modified. The stress applied on the specimen in the x direction was maintained nearly constant, while the stress applied on the specimen in the y direction was determined by intermediate stress ratio $b = (\sigma_2 - \sigma_3)/(\sigma_1 - \sigma_3)$. The normal and shear parallel bond strength of the spheres are set to final value of 1×10^8 N/m^2 at the beginning of this stage to allow bond breakage. To ensure a quasi-static condition in the numerical tests, an index I_{uf} proposed by Kuhn [43] and Ng [44] was used in this study. During all simulations, the values of I_{uf} remained a quite low value (less than 1.0%), which according to Kuhn [43] and Ng [44] corresponds to a quasi-static condition.

3. Macroscopic response

A series of numerical true triaxial tests were conducted under constant confining pressures ($\sigma_3 = 400$ kPa, 600 kPa, 800 kPa and 1000 kPa). The variation values of intermediate principle stress ratio b considered in this study are 0.0, 0.25, 0.50, 0.75 and 1.00, respectively. Figs. 3–5 show the typical macroscopic responses of crushable agglomerates with different b values.

The evolutions of stress ratio η versus axial strain are shown in Fig. 3. The stress ratio η is defined as follow:

$$\eta = \frac{q}{p'} \tag{9}$$

where $q = \sqrt{((\sigma_1 - \sigma_2)^2 + (\sigma_2 - \sigma_3)^2 + (\sigma_3 - \sigma_1)^2)/2}$, $p' = (\sigma_1 + \sigma_2 + \sigma_3)/3$, and σ_1, σ_2 and σ_3 are the major, intermediate, and minor effective stresses, respectively.

It is shown in Fig. 3(a) that η is initially independent on b, and quickly starts to depend on b values. An increase in b value at $\sigma_3 = 1000$ kPa leads to a decrease in the stress ratio η at the same axial strain. The effect of confining pressure σ_3 on η is shown in Fig. 3(b). It is clear that an increase in confining stress σ_3 at b = 0.5 results in a decrease in the stress ratio η at the same axial strain.

The relationships between volumetric strain and axial strain are shown in Fig. 4. As shown in Fig. 4(a), all specimens with different b values initially contract, and the volumetric strains decrease with increasing b values. When the axial strains reach nearly 2%, all specimens begin to expand until the end. During this stage, volumetric strains decrease with increasing b until $b \approx 0.50$ and subsequently increase as b increases. The evolution of volumetric strains under different confining stresses with b = 0.5 is shown in Fig. 4(b). The volumetric strains decrease as confining stress increases at the same axial strain. The stress-strain-volume relationships of the

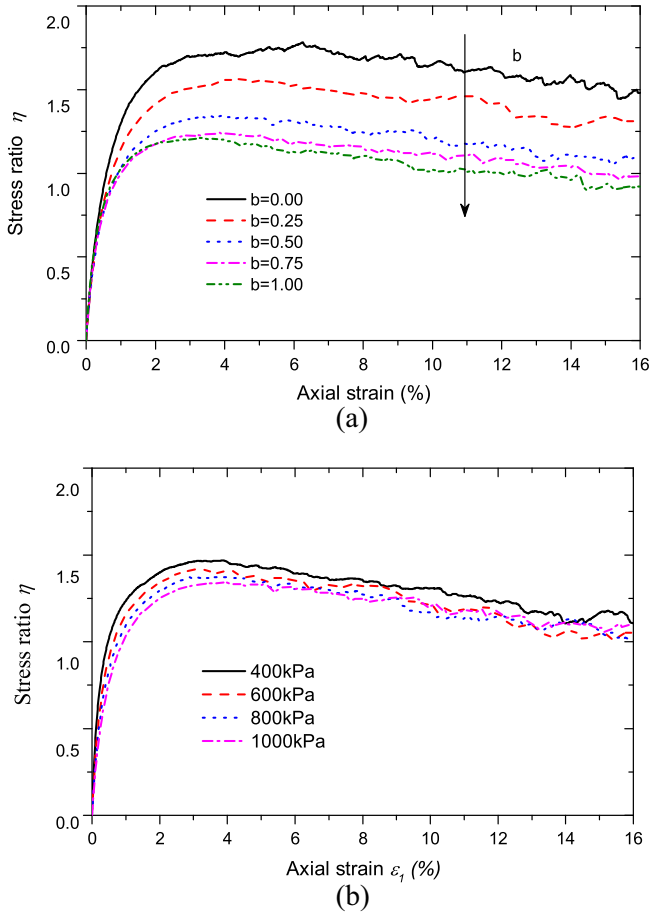

Fig. 3. The evolutions of stress ratio η versus Major principle strain:(a) stress ratio η with different b values ($\sigma_3 = 1000$ kPa); (b) stress ratio η with different σ_3 (b = 0.5).

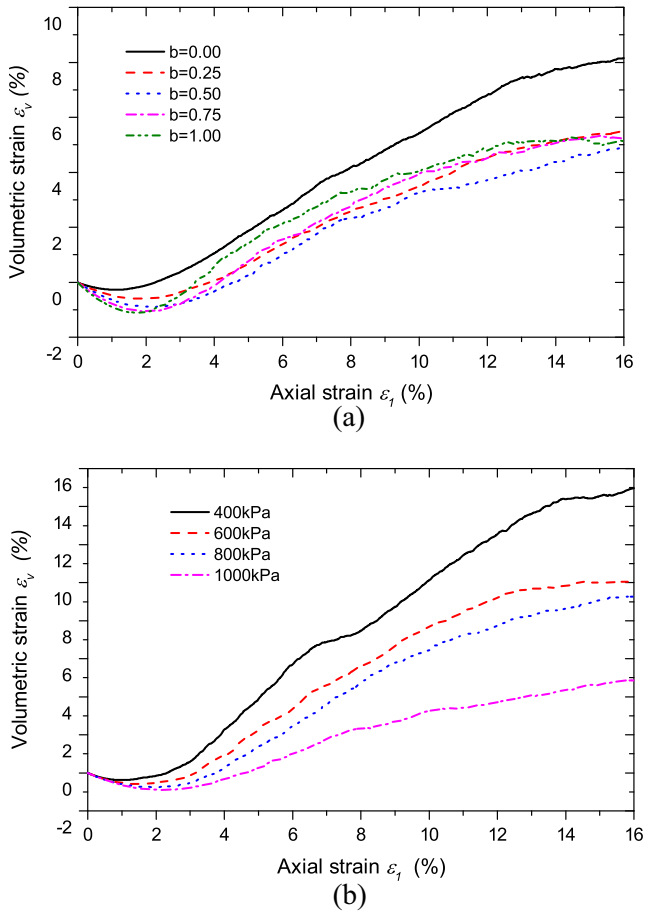

Fig. 4. The evolutions of volumetric strains versus Major principle strain: (a) volumetric strains with different b values ($\sigma_3 = 1000$ kPa); (b) volumetric strains with different σ_3 (b = 0.5).

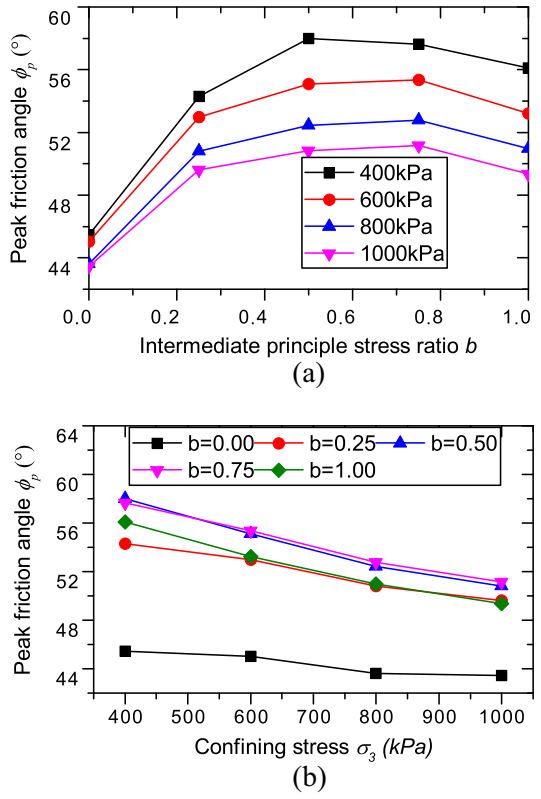

Fig. 5. Variations in peak friction angle ϕ_p with (a) b value; (b) minor principle stress σ_3.

numerical samples are consistent with those from true triaxial tests on crushable granular materials [21].

The peak friction angle ϕ_p is widely used to represent the variation of peak strength under generalized stress conditions. The peak friction angle ϕ_p is the maximum value of the mobilized friction angle ϕ_m during shearing, where the mobilized friction angle is defined as follows:

$$\phi_m = sin^{-1}\left(\frac{\sigma_1 - \sigma_3}{\sigma_1 + \sigma_3}\right) \tag{10}$$

The relationships of ϕ_p – b under different minor principle stresses σ_3 are shown in Fig. 5. Fig. 5 indicates that the peak friction angle ϕ_p depends on both the minor principle stress and b values. The peak friction angle first increases as b increases, and then when a certain b value is attained, the peak friction angle decreases with increasing b, as shown in Fig. 5(a). This trend is consistent with the experimental results in Xiao et al. [21]. The results presented in Fig. 5(b) illustrate that the peak friction angle decreases with increasing minor principle stress σ_3.

4. Influence of intermediate stress ratio *b* on particle breakage

4.1. Influence of b-values on bond breakage

Crushable agglomerates are comprised of elementary balls bonded together. If contact force acting on a parallel bond exceeds its strength, the bond breaks. As the number of broken bond increases, an agglomerate splits into fragments. So a larger number of broken bonds lead to a higher level of particle breakage. In this study, an index known as damage ratio [45] is applied to measure particle breakage in the assemble of crushable agglomerates. The damage ratio is defined as the number of broken bonds N_b divided by the number of total parallel bonds at the initial stage of shearing N_{b0}:

$$Damage\ ratio = \frac{N_b}{N_{b0}} \tag{11}$$

Fig. 6 shows the evolutions of the damage ratio with axial strain under different confining stresses. It can be seen in Fig. 6 that the damage ratio is basically zero initially until the axial strain reaches approximately 2%.After that, the bonds begin to break, and the bond breakage ratios increase rapidly with an increase in the axial strains. It is also shown in Fig. 6 that damage ratio increases with increasing principle stress ratio *b* at the same axial strain, which indicates that particle breakage of granular materials depends on the intermediate principle stress. This tendency agrees with the

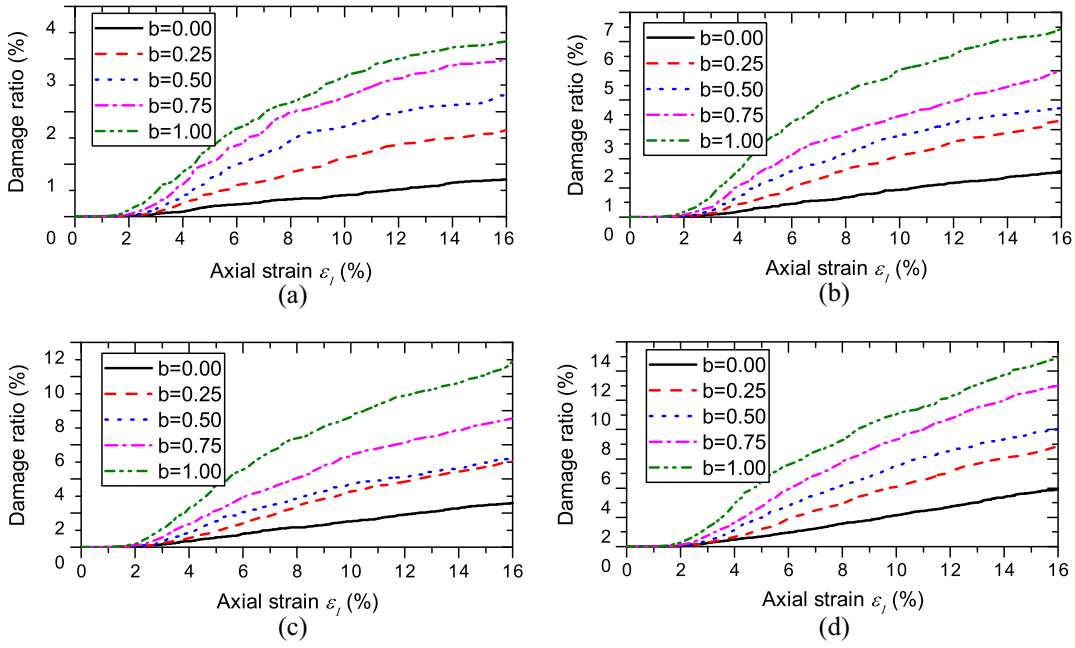

Fig. 6. The evolutions of damage ratio vs. axial strain: (a) 400 kPa; (b) 600 kPa; (c) 800 kPa; (d) 1000 kPa.

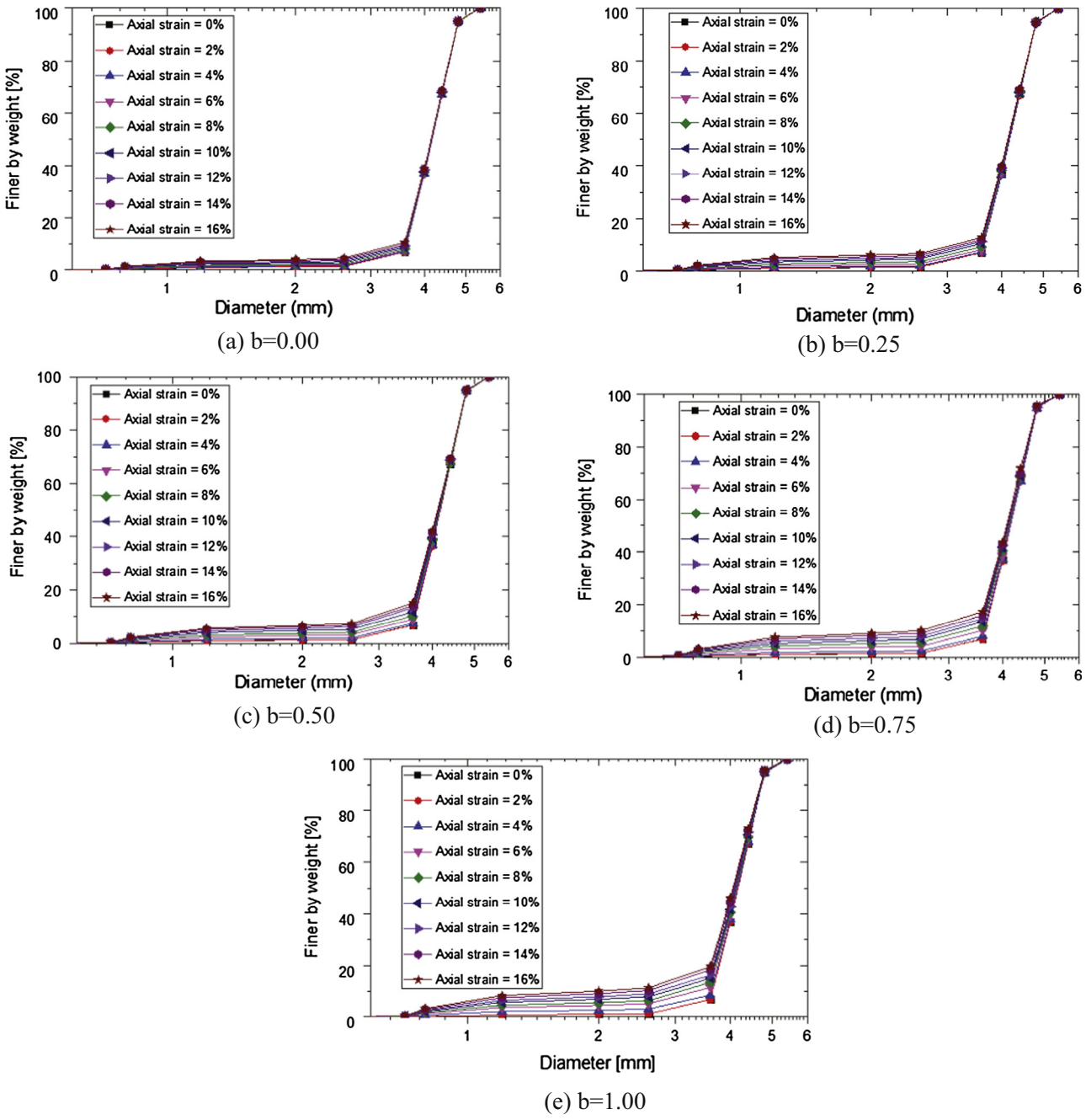

Fig. 7. The evolutions of particle size distribution of numerical specimens with different *b* values ($\sigma_3 = 1000$ kPa): (a) b = 0.00; (b) b = 0.25; (c) b = 0.50; (d) b = 0.75; (e) b = 1.00.

experimental results carried out on rockfill materials presented by Xiao et al. [21].

4.2. Influence of b-values on particle breakage

Tracking the evolution of PSD is one of the most difficult tasks in real triaxial test. However, it can be easily achieved in DEM simulations. To track the evolution of PSD, a method based on graph theory is employed in this study. In this method, elementary particles are deemed as vertexes, parallel bonds are deemed as edges, and each intact agglomerate is deemed as a contacted graph. If an agglomerate splits into several fragments, each fragment is deemed as a maximal connected subgraph. To track the evolution of PSD, one has to identify the fragments (subgraphs) first. The Warshell's algorithm is applied to identify the fragments (subgraphs) [46]. The Warshell's algorithm is an efficient algorithm to get the connectivity of undirected graph (broken agglomerate). The questions that how many numbers of fragments (subgraphs) there are and which fragment (subgraph) each elementary ball (vertex) belongs to can be easily solved by this algorithm.

After the fragments were identified, the diameters were calculated and assigned to the fragments. Since it is difficult to assign a single number (the grain diameter) to a 3-dimensional body, to capture both its size and shape [38], a simplified approach was used to calculate the diameters of the fragments:

$$D = d_{max} + 2d_e \tag{12}$$

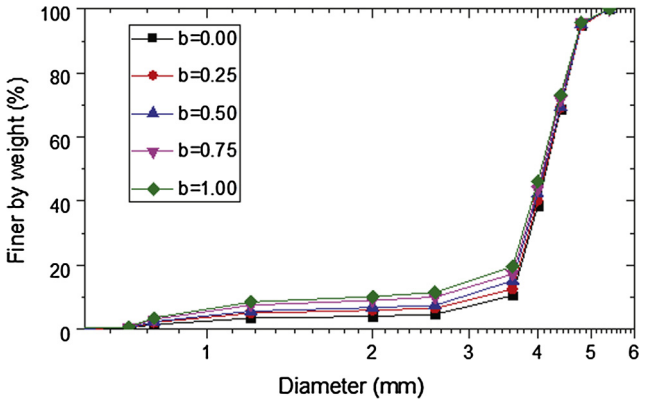

Fig. 8. Particle size distribution at axial strain 16% for different b values ($\sigma_3 = 1000$ kPa).

where d_{max} is the longest distance between centers of two elementary spheres in the fragments, and d_e is the radius of the elementary sphere in the fragments. A description of this PSD tracking method is given as follows:

(1) Create an array to store the mass of fragments in a specific range of particle diameters, and set all items of the array to be zero at the beginning of the analysis.
(2) For each agglomerate, the Warshell's algorithm is first applied to identify the number of its fragments and to determine to which fragment each elementary ball belongs.
(3) After that, create a table for each fragment to store the IDs of its elementary balls.
(4) Calculate the diameters of each fragment, and determine which diameter range it belongs to, then calculate its mass and add it to the corresponding items of the PSD array.
(5) After all fragments of an agglomerate is calculated, delete the tables created in step (3).
(6) Traverse all agglomerates and calculate their PSD respectively and get the whole PSD of the specimen.

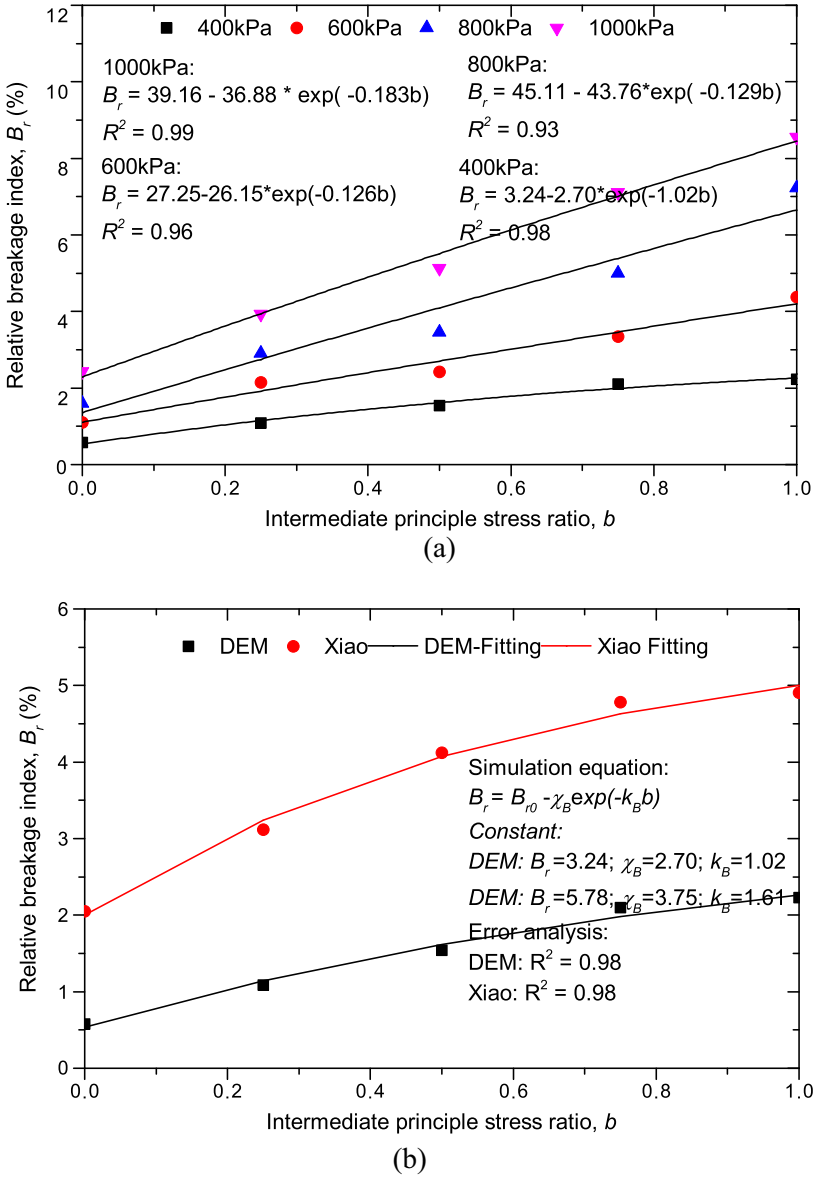

Fig. 9. Influence of b values on B_r: (a) the relationship of B_r and b-values; (b) comparison between experimental and DEM simulation results.

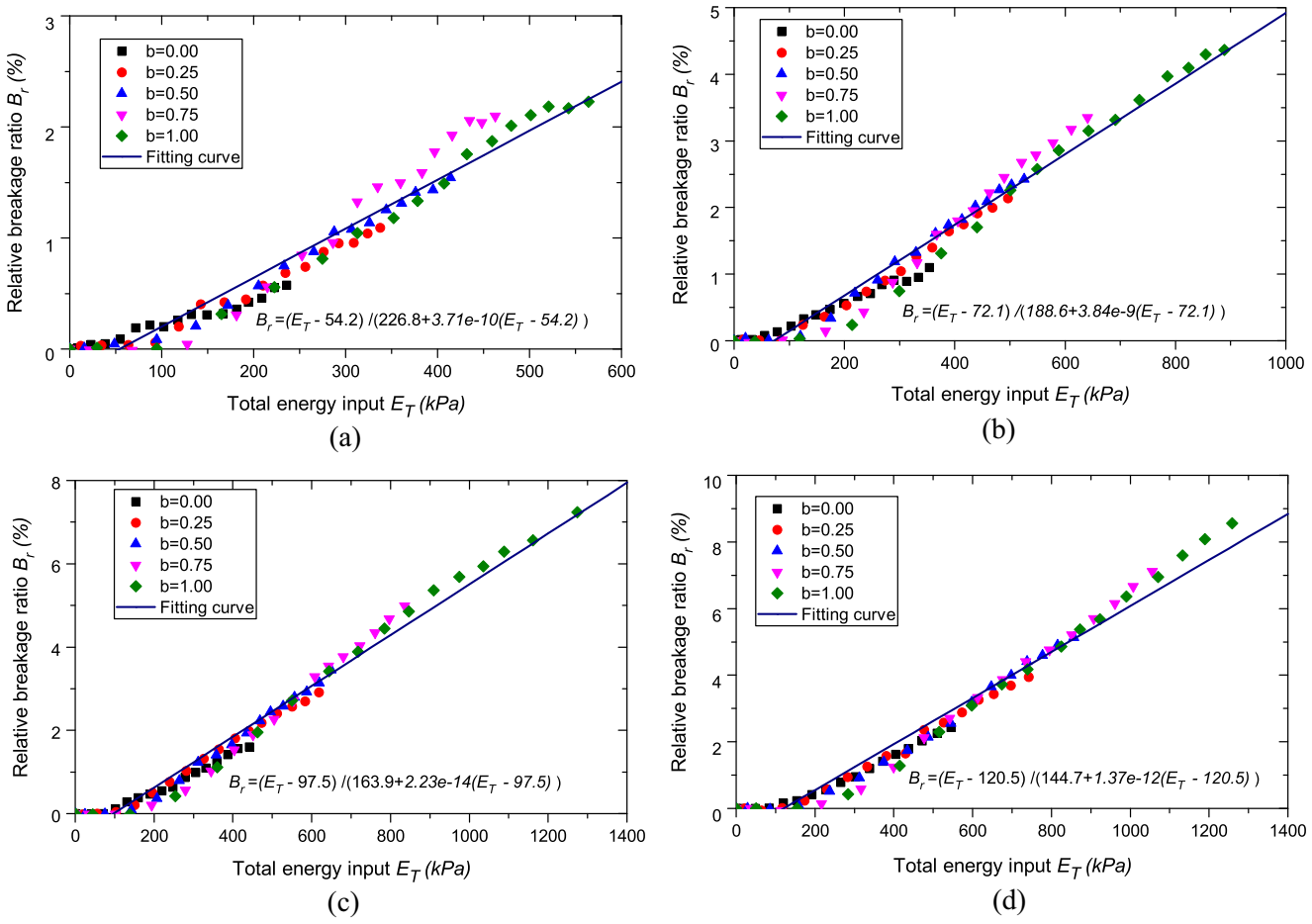

Fig. 10. The relationships between B_r and E_T: (a) 400 kPa; (b) 600 kPa; (c) 800 kPa; (d) 1000 kPa.

Fig. 7 presents the evolutions of PSDs with different b-values at a confining stress of $\sigma_3 = 1000$ kPa. As shown in Fig. 7, there is no significant change in the PSDS at small strains. Afterwards the PSDs change in a stable pattern, which is consistent with the observations of bond breakage. This implies that the method employed in this study is capable of tracking the PSDs. It can also be seen that the major changes of PSDs in all conditions occur in relatively small diameter areas. This means that smaller particles break first in all conditions. This behavior agrees with experimental results [47] and other DEM simulation results [38], and has been theoretically explained [6].

To investigate the effect of b-values on the evolution of the PSDs, the PSDs with different b values at axial strain $\varepsilon_1 = 16\%$ are presented in Fig. 8. It is clear that the evolutions of PSDs depend on the intermediate principle stress ratio b, and an increase in the b-values can lead to an increase in the change of the PSDs. This trend agrees with the observation of laboratory tests presented by Xiao et al. [21].

4.3. Relationship between particle breakage and b value

Different particle breakage indices have been proposed to represent the extent of particle breakage. Among them, Hardin's particle breakage factor B_r is believed to be the most appropriate and is widely used by other researchers. In this study, B_r is selected as the reference of particle breakage.

As stated by Xiao et al. [21], the relationship between the b-value and the relative breakage index B_r can be given as

$$B_r = B_{r0} - \chi_B e^{-k_B b} \tag{13}$$

where B_r is the relative breakage index proposed by Hardin, B_{r0}, χ_B and k_B are material constants.

To compare with the observation presented by Xiao et al. [21], the Hardin's relative breakage indices B_r at an axial strain of 16% are selected and analyzed using Eq. (13).The values of B_r at an axial strain of 16% for all tests are plotted against b-values as shown in Fig. 9. It can be seen in Fig. 9(a) that the relationships between the b-values and the relative breakage indices B_r under different confining stresses can be well represented by Eq. (13). The experimental and DEM simulation results under the same confining stress of 400 kPa are compared as shown in Fig. 9(b). It appears that both of them have the same trend.

5. Relationship between particle breakage and energy input

For a specimen in conventional triaxial test, the total energy input per unit volume is the sum of energy input during the isotropic compression and shearing phases

$$E_T = E_C + E_S = \sum_{SOT}^{BOS} \bar{\sigma}_c \cdot \dot{\varepsilon}_v + \left[\sum_{BOS}^{EOS} (\sigma_1 - \sigma_3) \cdot \dot{\varepsilon}_a + \sum_{BOS}^{EOS} \sigma_c \cdot \dot{\varepsilon}_v \right] \tag{14}$$

in which E_C = energy input during isotropic compression; E_S = energy input during shearing; σ_c = finial confining pressure; $\bar{\sigma}_c$ = average confining pressure over increment; $\dot{\varepsilon}_v$ = volumetric strain increment; $(\sigma_1 - \sigma_3)$ = average stress difference over increment; $\dot{\varepsilon}_a$ = axial strain increment; SOT = start of test; EOS = end of shearing; and BOS = beginning of shearing.

In this study, particle breakage during isotropic compression was not considered to save computing time, so $E_T = E_s$.

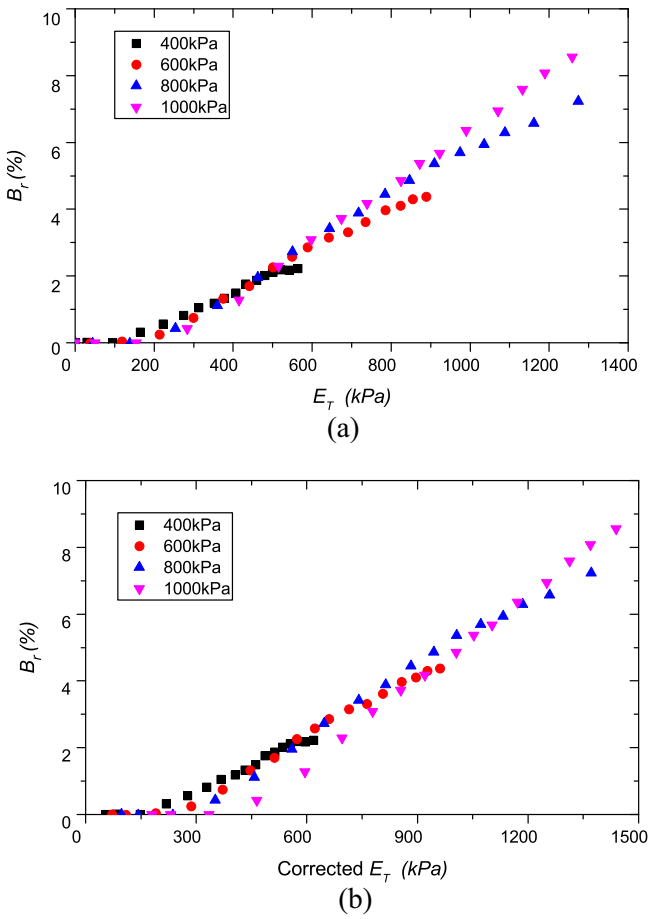

Fig. 11. The relationships between B_r and energy input under different initial confining stresses with b = 1.00: (a) B_r versus E_T; (b) B_r versus Corrected E_T.

Furthermore, Eq. (14) is inapplicable to calculate total energy input in true triaxial test. So the total energy input adopted in this study is rewritten as

$$E_T = E_S = \sum_{BOS}^{EOS} (\sigma_x \cdot y \cdot z \cdot \mathrm{d}x + \sigma_y \cdot x \cdot z \cdot \mathrm{d}y + \sigma_z \cdot x \cdot y \cdot \mathrm{d}z) \frac{1}{x \cdot y \cdot z} \tag{15}$$

in which σ_x, σ_y and σ_z are stresses in x, y, z direction, respectively; x, y and z are lengths of specimen in x, y, z direction, respectively; and dx, dy and dz are length increments in x, y and z direction, respectively.

The relationships between total energy input per unit volume E_T and relative breakage ratio B_r under different confining pressures are presented in Fig. 10. It can be seen that there are two stages in these curves. In the first stage at small input energy, particle breakage is negligible; after the energy input attains certain value, particle breakage begins to increase with an increase in the input energy. The results agree well with the experimental observations presented by Karimpour and Lade [2]. More importantly, it can be seen that the energy input is closely related to particle breakage index B_r, independent of the intermediate principle stress ratio. The relationship may be very well approximated by some hyperbolic equation, as shown in Fig. 10:

$$B_r = \frac{E_T - E_{th}}{c + d(E_T - E_{th})} \tag{16}$$

in which E_T is the total energy input per unit volume of the specimen; c and d are hyperbolic curve-fit parameters;and E_{th} is the threshold energy input that initiates particle breakage [48]. When $E_{th} = 0$, Eq. (16) becomes

$$B_r = \frac{E_T}{c + dE_T} \tag{17}$$

Similar relationships have been observed from conventional triaxial tests in many previous studies [1,2,23,24,32,41].

Apparently, there exists a certain relationship between the particle breakage and energy input that is independent on loading path. The degrees of curvature of the fitting curves are determined by parameter d in Eq. (16), and it is obvious that the values of parameter d in Eq. (16) are very small, which means the relationship between the particle breakage and energy input is basically linear at low to medium level of energy input. It is also found that E_{th} increases with an increase in the confining stress in the numerical tests.

For the sake of computational efficiency, agglomerates were only allowed to break at the shearing stage in this study, and the energy input during isotropic compression is also not considered. This assumption is quite different from actual tests, since energy input during isotropic compression is not negligible, and particle breakage may also occur in this stage. This difference may lead to discrepancy between DEM simulation result and experimental result when the effect of initial confining pressure is taken into account.

Fig. 11(a) presents the relationships between B_r and total energy input under different initial confining pressures with b = 1.00. It can be seen that the relationship is slightly influenced by the confining pressure, but in laboratory tests, the relationship between B_r and total input energy is found to be independent on initial confining pressures [20,23].

This inconsistency maybe attributed to the simplified procedure used in this study. It is assumed that no particle breakage occurs during isotropic compression for the numerical specimens investigated in this study, but the energy input during this stage is different with different confining pressures. The larger the confining pressure, the larger the input energy. This means that the horizontal coordinates of the curves in Fig. 11(a) should actually be larger if taking into account the energy input during isotropic compression, and the increase is larger for higher confining pressure. An attempt has been made by horizontally translating the curves in Fig. 11(a) according a certain gradient. The difference of translation is obtained as the difference in the values of E_{th} in Fig. 10. The resulted curves then follow very similar trend and the influence of confining pressure ceases to exist, as shown in Fig. 11(b).

6. Conclusions

Particle breakage of granular materials under true triaxial tests was investigated in this study using 3D DEM simulation considering both the influences of initial confining stress and intermediate principle stress. To simulate realistic fracture behavior of a single granular particle, the crushable agglomerate method proposed by Robertson and Bolton [33] was modified and applied. 30 random created agglomerate were tested using uniaxial compression tests to examine the validity of the simulation method. Then a series of true triaxial compression tests were carried out to study the effects of both initial confining stress and intermediate principle stress on the macroscopic responses and particle breakage. Particularly, the relationship between particle breakage and total energy input was investigated considering the influence of different loading paths.

The main conclusions are summarized as follows:

(1) The result of single particle compression tests shows that the statistical distribution of the strength of crushable agglomerates, in line with previous studies on actual granular particles, is in good agreement with the Weibull's distribution.
(2) The peak friction angle of granular materials at a specific confining stress σ_3 increased to a peak value and then decreased with an increase in the *b*-value, and the peak friction angle at a specific *b*-value decreased with an increase in σ_3, which are in good agreement with previous experimental findings.
(3) Two particle breakage indices, damage ratio and Hardin's relative breakage index, were used to study the particle breakage of granular materials. Both damage ratio and Hardin's relative breakage index B_r increased with an increasing *b* value at a specific confining stress σ_3.The relationship between particle breakage and intermediate stress is consistent with the experimental results by Xiao et al. [21].
(4) The relationship between particle breakage indices and total energy input of granular materials was independent on the b-value. The relationship could be fitted very well by a hyperbolic equation.

References

[1] Lade PV, Yamamuro JA, Bopp PA. Significance of particle crushing in granular materials. J Geotech Eng 1996;122(4):309–16.
[2] Karimpour H, Lade PV. Time effects relate to crushing in sand. J Geotech Geoenviron 2010;136(9):1209–19.
[3] Bolton M, Nakata Y, Cheng Y. Micro-and macro-mechanical behaviour of DEM crushable materials. Geotechnique 2008;58(6):471–80.
[4] Jaeger J. Failure of rocks under tensile conditions. Int J Rock Mech Mining Sci Geomech Abstr 1967;5:219–27 [Elsevier].
[5] Lee D-M. Angles of friction of granular fills. University of Cambridge; 1992.
[6] McDowell G, Bolton M. On the micromechanics of crushable aggregates. Geotechnique 1998;48(5):667–79.
[7] McDowell G, Amon A. The application of Weibull statistics to the fracture of soil particles. Soil Found 2000;40(5):133–41.
[8] Nakata A, Hyde M, Hyodo H, Murata. A probabilistic approach to sand particle crushing in the triaxial test. Geotechnique 1999;49(5):567–83.
[9] Wang W, Coop M. An investigation of breakage behaviour of single sand particles using a high-speed microscope camera. Geotechnique 2016:1–15.
[10] Zhao B, Wang J, Coop M, Viggiani G, Jiang M. An investigation of single sand particle fracture using X-ray micro-tomography. Geotechnique 2015;65(8):625–41.
[11] Oldecop LA, Alonso Pérez de Agreda E. Theoretical investigation of the time-dependent behaviour of rockfill; 2007.
[12] Frossard E, Hu W, Dano C, Hicher P. Rockfill shear strength evaluation: a rational method based on size effects. Geotechnique 2012;62(5):415.
[13] de Bono JP, McDowell GR. DEM of triaxial tests on crushable sand. Granul Matter 2014;16(4):551–62.
[14] Ciantia MO, Arroyo M, Calvetti F, Gens A. An approach to enhance efficiency of DEM modelling of soils with crushable grains. Geotechnique 2015;65(2):91–110.
[15] Tapias M, Alonso E, Gili J. A particle model for rockfill behaviour. Geotechnique 2015;65(12):975–94.
[16] Marsal RJ. Large-scale testing of rockfill materials. J Soil Mech Found Div 1967;93(2):27–43.
[17] Indraratna B, Wijewardena L, Balasubramaniam A. Large-scale triaxial testing of greywacke rockfill. Geotechnique 1993;43(1):37–51.
[18] Varadarajan A, Sharma K, Venkatachalam K, Gupta A. Testing and modeling two rockfill materials. J Geotech Geoenviron 2003;129(3):206–18.
[19] Indraratna B, Thakur PK, Vinod JS. Experimental and numerical study of railway ballast behavior under cyclic loading. Int J Geomech 2009;10(4):136–44.
[20] Zhang B-Y, Jie Y-X, Kong D-Z. Particle size distribution and relative breakage for a cement ellipsoid aggregate. Comput Geotech 2013;53:31–9.
[21] Xiao Y, Liu H, Chen Y, Chu J. Influence of intermediate principal stress on the strength and dilatancy behavior of rockfill material. J Geotech Geoenviron 2014;140(11):04014064.
[22] Xiao Y, Liu H, Chen Y, Jiang J. Strength and deformation of rockfill material based on large-scale triaxial compression tests. II: Influence of particle breakage. J Geotech Geoenviron 2014;140(12):04014071.
[23] Liu J, Zou D, Kong X, Liu H. Stress-dilatancy of Zipingpu gravel in triaxial compression tests. Sci China Technol Sci 2016;59(2):214–24.
[24] Kong X, Liu J, Zou D, Liu H. Stress-dilatancy relationship of Zipingpu gravel under cyclic loading in triaxial stress states. Int J Geomech 2016:04016001.
[25] Hardin BO. Crushing of soil particles. J Geotech Eng 1985;111(10):1177–92.
[26] Xiao Y, Sun Y, Hanif KF. A particle-breakage critical state model for rockfill material. Sci China Technol Sci 2015;58(7):1125–36.
[27] Xiao Y, Liu H, Ding X, Chen Y, Jiang J, Zhang W. Influence of particle breakage on critical state line of rockfill material. Int J Geomech 2015;16(1):04015031.
[28] Einav I. Breakage mechanics—Part I: Theory. J Mech Phys Solids 2007;55(6):1274–97.
[29] Varadarajan A, Sharma K, Abbas S, Dhawan A. Constitutive model for rockfill materials and determination of material constants. Int J Geomech 2006;6(4):226–37.
[30] Daouadji A, Hicher P-Y, Rahma A. An elastoplastic model for granular materials taking into account grain breakage. Eur J Mech A-Solid 2001;20(1):113–37.
[31] Daouadji A, Hicher PY. An enhanced constitutive model for crushable granular materials. Int J Numer Anal Met 2010;34(6):555–80.
[32] Liu H, Zou D. Associated generalized plasticity framework for modeling gravelly soils considering particle breakage. J Eng Mech 2012;139(5):606–15.
[33] Robertson D, Bolton MD. DEM simulations of crushable grains and soils. Powders Grains 2001;2001:623–6.
[34] Cheng YP, Nakata Y, Bolton MD. Discrete element simulation of crushable soil. Geotechnique 2003;53(7):633–41.
[35] Cheng YP, Bolton MD, Nakata Y. Crushing and plastic deformation of soils simulated using DEM. Geotechnique 2004;54(2):131–41.
[36] Kwok CY, Bolton MD. DEM simulations of soil creep due to particle crushing. Geotechnique 2013;63(16):1365–76.
[37] Wang JF, Yan HB. On the role of particle breakage in the shear failure behavior of granular soils by DEM. Int J Numer Anal Met 2013;37(8):832–54.
[38] Laufer I. Grain crushing and high-pressure oedometer tests simulated with the discrete element method. Granul Matter. 2015;17(3):389–412.
[39] Huang J, Xu S, Hu S. Effects of grain size and gradation on the dynamic responses of quartz sands. Int J Impact Eng 2013;59:1–10.
[40] Sazzad MM, Suzuki K. Density dependent macro-micro behavior of granular materials in general triaxial loading for varying intermediate principal stress using DEM. Granul Matter 2013;15(5):583–93.
[41] Liu H, Zou D, Liu J. Constitutive modeling of dense gravelly soils subjected to cyclic loading. Int J Numer Anal Met 2014;38(14):1503–18.
[42] Davidge RW. Mechanical behaviour of ceramics. CUP Archive; 1979.
[43] Kuhn MR. OVAL and OVALPLOT: Programs for analyzing dense particle assemblies with the discrete element method. Reporte de investigación; 2006.
[44] Ng TT. Input parameters of discrete element methods. J Eng Mech 2006;132(7):723–9.
[45] Thornton C, Ciomocos M, Adams M. Numerical simulations of agglomerate impact breakage. Powder Technol 1999;105(1):74–82.
[46] Warshall S. A theorem on boolean matrices. J ACM 1962;9(1):11–2.
[47] Chuhan FA, Kjeldstad A, Bjørlykke K, Høeg K. Porosity loss in sand by grain crushing-experimental evidence and relevance to reservoir quality. Mar Petrol Geol 2002;19(1):39–53.
[48] Liu J, Liu H, Zou D, Kong X. Particle breakage and the critical state of sand: By Ghafghazi, M., Shuttle, DA, DeJong, JT, 2014. Soil Found 54 (3), 451–461. Soil Found 2015;1(55):220–2.